Research paper

In-situ nickel(II) complexes of 3-(dimethylamino)-1-propylamine based Schiff base ligands: Structural, electrochemical, biomolecular interaction and antimicrobial properties

Arumugam Jayamani, Soundarajan Nagasubramanian, Vijayan Thamilarasan, Stephen O. Ojwach, Gopalakrishnan Gopu, Nallathambi Sengottuvelan

PII: S0020-1693(18)30847-8
DOI: https://doi.org/10.1016/j.ica.2018.07.018
Reference: ICA 18364

To appear in: *Inorganica Chimica Acta*

Received Date: 1 June 2018
Revised Date: 10 July 2018
Accepted Date: 10 July 2018

Please cite this article as: A. Jayamani, S. Nagasubramanian, V. Thamilarasan, S.O. Ojwach, G. Gopu, N. Sengottuvelan, *In-situ* nickel(II) complexes of 3-(dimethylamino)-1-propylamine based Schiff base ligands: Structural, electrochemical, biomolecular interaction and antimicrobial properties, *Inorganica Chimica Acta* (2018), doi: https://doi.org/10.1016/j.ica.2018.07.018

In-situ nickel(II) complexes of 3-(dimethylamino)-1-propylamine based Schiff base ligands: Structural, electrochemical, biomolecular interaction and antimicrobial properties

Arumugam Jayamani[a,b], Soundarajan Nagasubramanian[a], Vijayan Thamilarasan[a,c], Stephen O. Ojwach[b], Gopalakrishnan Gopu[a], Nallathambi Sengottuvelan[a]*

[a]Department of Industrial Chemistry, School of Chemical Sciences, Alagappa University, Karaikudi – 630003, Tamilnadu, India

[b]Department of Chemistry School of Chemistry and Physics, University of KwaZulu-Natal, Private Bag X01, Scottsville, Pietermaritzburg 3209, South Africa

[c]Department of Chemistry and Nano Science, Ewha Womans University, Seoul-120 750, Republic of Korea.

Abstract

Five new di-Schiff base nickel(II) complexes (**1**–**5**) of salen type ligands were synthesized *in-situ* by condensation of 3-(dimethylamino)-1-propylamine with 2-hydroxybenzaldehyde, 2-hydroxy-5-methyl benzaldehyde, 2-hydroxy-5-bromo benzaldehyde, 2-hydroxy-5-nitrobenzaldehyde and 2-hydroxy-1-naphthaldehyde to obtain $\mathbf{L^1}$-$\mathbf{L^5}$, respectively and complexed with nickel chloride. Single crystal X-ray diffraction studies of complexes **1** and **5** showed a distorted octahedral and distorted square-planar geometry, respectively around nickel atoms. The cyclic voltammetry of complexes **1**–**5** showed redox peaks near cathodic and anodic regions assignable to the Ni^{2+}/Ni^{+} and Ni^{2+}/Ni^{3+} redox couples, respectively. The binding studies of complexes with calf thymus DNA (ctDNA) showed an intercalation mode of binding. The nuclease activity of the complexes with pBR322 plasmid DNA showed efficient oxidative cleavage by the formation of singlet oxygen species in presence of H_2O_2. All nickel(II) complexes were found to have greater zone inhibition diameter when

analyzed for antimicrobial property against four bacterial species and two human pathogenic fungal species.

Keywords: Nickel(II) complexes; Single crystal, Oxidative cleavage, Antimicrobial activity

1. Introduction

The salen type di-Schiff base complexes of transition metal ions showed a continuous interest and were extensively studied over past few decades due to their stability, chelating properties, fascinating structural features, efficient electrochemical and magnetic properties, and biological applications as metalloenzymes [1–3]. They play a vital role in the field of bioinorganic chemistry as they can easily form stable complexes [4,5]. The transition metal complexes of Schiff bases derived from aromatic compounds containing nitrogen and oxygen atoms are of current interest as simple structural models of biological systems [6–9]. Among the transition metal ions, the study of nickel compounds is of great interest in various aspects of chemistry [10,11]. In general, the reaction of salen or related ligands with Ni(II) yields complexes in which the deprotonated, di-negative Schiff base acts as a tetradentate chelating ligand [12–14]. However, in some cases, it has been found that the oxygen atoms of the Schiff base are not deprotonated in case of having bulky substituents [15]. In this work, an attempt was made to study the steric and electronic effect of ligand substituent on the geometry and biomolecular interaction of the Ni(II) complexes.

In the present work, nickel(II) complexes [Ni($\mathbf{L}^1$)$_2$] (**1**), [Ni($\mathbf{L}^2$)$_2$] (**2**), [Ni($\mathbf{L}^3$)$_2$] (**3**), [Ni($\mathbf{L}^4$)$_2$] (**4**) and [Ni($\mathbf{L}^5$)$_2$]Cl$_2$ (**5**) were synthesized with Schiff base ligands prepared by *in-situ* condensation of 3-(dimethylamino)-1-propylamine with different aldehydes. Some of these compounds and similar complexes were previously reported by Sacconi et al, synthesized from bis(salicylaldehyde) nickel(II) complexes studies and studied their four/five/six coordination [16-18]. The DNA binding and cleavage ability of all the nickel(II)

complexes were evaluated using calf thymus DNA (ctDNA) and plasmid pBR322 DNA, respectively. The antimicrobial properties of the complexes were evaluated against four bacteria and two pathogenic fungi.

2. Experimental

2.1. Materials

All the chemicals used were of analytical grade and were used as received without any further purification. The amine, 3-(dimethylamino)-1-propylamine and aldehydes 2-hydroxybenzaldehyde, 2-hydroxy-5-methyl benzaldehyde, 2-hydroxy-5-bromo benzaldehyde, 2-hydroxy-5-nitrobenzaldehyde, 2-hydroxy-1-naphthaldehyde were obtained from Alfa Aesar, (India). The calf thymus and plasmid DNA's were purchased from SRL (India), Tris–HCl, Tris–base and NaCl were purchased from Merck (India).

2.2. Instrumentation

The UV-Visible spectra were recorded on a Shimadzu UV-3101PC spectrophotometer. FT-IR spectra were recorded in the 4000– 400 cm^{-1} regions using KBr pellets on a Bruker EQUINOX 55 spectrometer. The elemental composition of the complexes was evaluated on an Elementar Vario MACRO cube elemental analyzer. The electron spray ionization mass spectra (positive mode) were recorded on an Aligent 6520 Q-T mass spectrometer (Central Drug Research Institute, Lucknow, India). The fluorescence quenching experiment of DNA-bound to EB for the synthesized complexes were recorded on an Elico SL-174 spectrofluorometer. The redox potential of the complexes was measured on a Biologic CHI604D electrochemical analyzer using a three-electrode cell under nitrogen atmosphere where a glassy carbon, Ag/AgCl and a platinum wire were used as working electrode, a reference electrode and the auxiliary electrode, respectively. The complexes (1 mM) in dimethylformamide with 0.1 M supporting electrolyte, tetra(n-butyl) ammonium

perchlorate were used for cyclic voltammetry studies. All the solvents were purified according to standard procedures.

2.3. Synthesis of *in-situ* nickel (II) complexes

2.3.1. $[Ni(L^1)_2]$(**1**): To a solution of $NiCl_2.6H_2O$ (0.24 g, 1 mM) in methanol (25 mL), 2-hydroxybenzaldehyde (0.24 g, 2 mM) in methanol was added slowly with constant stirring, then 3-(dimethylamino)-1-propylamine (0.20 g, 2 mM), was added to the reaction mixture and the content was stirred at room temperature for three hours followed by reflux for about two hours. The green coloured precipitate formed was dried and recrystallized in acetonitrile to obtain green crystals after a few days. Yield: 0.51 g, 56 %. m.p.: 201 °C (dec). Anal. data for $C_{24}H_{34}N_4O_2Ni$: Calc. (%): C, 61.43; H, 7.25; N, 11.94; Ni, 12.51; Found (%): C, 61.37; H, 7.24; N, 11.86; Ni, 12.43; FT–IR (ν, cm^{-1}) (KBr Disc): 1636(ν C=N), 565(ν Ni-O), 492(ν Ni-N); UV-Vis [λ_{max}/nm (ε_{max}/ mol^{-1} cm^{-1})]: 272 (60910), 310 (33460), 376 (56060), 538 (15), 745 (10); Molar conductivity (Λ_m/Scm^2mol^{-1}) in acetonitrile 15.

Other nickel(II) complexes **1**-**5** were synthesized by a procedure similar to that of complex **1**.

2.3.2. $[Ni(L^2)_2]$ (**2**): 2-hydroxy-5-methyl benzaldehyde (0.27 g, 2 mM), $NiCl_2.6H_2O$ (0.24 g, 1 mM), 3-(dimethylamino)-1-propylamine (0.20 g, 2 mM). The greenish yellow coloured precipitate obtained was filtered and dried. Yield: 0.56 g, 60 %; m.p.: 188 °C (dec). Anal. data for $C_{26}H_{38}N_4O_2Ni$ Calc. (%): C, 62.79; H, 7.65; N, 11.27; Ni, 11.80; Found (%): C, 62.73; H, 7.74; N, 11.14; Ni, 11.67; FT–IR (ν, cm^{-1}) (KBr Disc): 1629(ν C=N), 556(ν Ni-O), 468(ν Ni-N); UV-Vis [λ_{max}/nm (ε_{max}/ mol^{-1} cm^{-1})]: 273(6685), 388(6023), 653(19), 695(18); Molar conductivity ($\Lambda_m Scm^{-1}mol^{-1}$) in acetonitrile 16.

2.3.3. $[Ni(L^3)_2]$ (**3**): 2-hydroxy-5-bromo benzaldehyde (0.42 g, 2 mM), $NiCl_2.6H_2O$ (0.24 g, 1 mM), 3-(dimethylamino)-1-propylamine (0.20 g, 2 mM). The green coloured precipitate obtained was filtered and dried. Yield: 0.64 g, 60 %; m.p.: 199 °C (dec). Anal. data for $C_{24}H_{32}Br_2N_4O_2Ni$ Calc. (%): C, 45.97; H, 5.14; N, 8.94; Ni, 9.36; Found (%): C, 45.9; H,

5.18; N, 8.81; Ni, 9.25; FT–IR (ν, cm^{-1}) (KBr Disc): 1625(ν C=N), 570(ν Ni-O), 490(ν Ni-N); UV-Vis [λ_{max}/nm (ε_{max}/ mol^{-1} cm^{-1})]: 275 (6665), 387 (6275), 635 (10), 699 (10); Molar conductivity ($\Lambda_m Scm^{-1}mol^{-1}$) in acetonitrile 12.

2.3.4. $[Ni(L^4)_2]$ (**4**): 2-hydroxy-5-nitrobenzaldehyde (0.33 g, 2 mM), $NiCl_2.6H_2O$ (0.24 g, 1 mM), 3-(dimethylamino)-1-propylamine (0.20 g, 2 mM). The green coloured precipitate obtained was filtered and dried. Yield: 0.65 g, 65 %; m.p.: 183 °C (dec.) Anal. data for $C_{24}H_{32}N_6O_6Ni$ Calc. (%): C, 51.54; H, 5.72; N, 15.03; Ni, 10.50; Found (%): C, 51.48; H, 5.64; N, 14.92; Ni, 10.30; FT–IR (ν, cm^{-1}) (KBr Disc): 1625(ν C=N), 568(ν Ni-O), 464(ν Ni-N); UV-Vis [λ_{max}/nm (ε_{max}/ mol^{-1} cm^{-1})]: 288 (7920), 404 (58180), 585 (19), 740(3); Molar conductivity ($\Lambda_m Scm^{-1}mol^{-1}$) in acetonitrile 14; ESI-MS (CH_3CN) *m/z* (%): 558.7(6) $[Ni(\mathbf{L^4})_2+H]^+$, 369.2(38), 300.9(76), 251.8(32), 148.6(65), 113.7(100)

2.3.5. $[Ni(L^5)_2]Cl_2$ (**5**): 2-hydroxy-1-naphthaldehyde (0.34 g, 2 mM), $NiCl_2.6H_2O$ (0.24 g, 1 mM), 3-(dimethylamino)-1-propylamine (0.20 g, 2 mM). The green coloured precipitate formed was dried and recrystallized in acetonitrile to obtain green crystals by slow evaporation after few days. Yield: 0.61g, 60 %; m.p.: 191 °C (dec); Anal. data for $C_{32}H_{40}N_4O_2NiCl_2$ Calc. (%): C, 59.84; H, 6.28; N, 8.72; Ni, 9.14; Found (%): C, 59.40; H, 6.41; N, 8.61; Ni, 9.16; FT–IR (ν, cm^{-1}) (KBr Disc): 3336(ν O-H), 2980(s), 1621(ν C=N), 568(ν Ni-O), 496(ν Ni-N); UV-Vis [λ_{max}/nm (ε_{max}/ mol^{-1} cm^{-1})]: 277 (24030), 305 (16150), 404 (11806), 635 (10); Molar conductivity ($\Lambda_m Scm^{-1}mol^{-1}$) in acetonitrile 122.

2.4. Single crystal XRD

The in-situ Schiff base nickel complexes **1** and **5** were obtained as green crystals suitable for X-ray diffraction studies by recrystallization using acetonitrile solvent. The X-ray diffraction analysis of the complexes was carried out on Bruker SMART APEX-II CCD diffractometer, using a single crystal with different dimensions with graphite monochromatized Mo-Kα radiation (λ = 0.71073 Å). Data reduction and corrections for

absorption and decomposition were achieved using the SAINT/X-PREP software [19]. The structure was solved using the direct methods and successive Fourier difference synthesis thermal parameters for all non-hydrogen atoms (SHELXL-97) and all nonhydrogen atoms were refined anisotropically by full-matrix least-square procedures. Hydrogen atoms were added theoretically and refined with riding model position parameters and fixed isotropic thermal parameters.

2.5. DNA binding and cleavage studies

The ctDNA was used in binding experiments due to greater similarity with that of mammalian DNA, also at high molecular weights, the impurity due to the presence of protein can be easily identified. The UV absorption spectral method was used to study the binding ability of synthesized nickel(II) complexes with ctDNA. The stock solution of ctDNA was prepared in 5 mM Tris–HCl/ 20 mM NaCl buffer (pH = 7.2), stored at 4 °C and used within 4 days. The solution of ctDNA gave a ratio of UV absorbance at 260 nm and 280 nm, A_{260}/ A_{280}, of 1.8-1.9, indicating that the ctDNA was sufficiently free of proteins. Absorption titration experiments were performed by varying the DNA concentration while keeping the complex concentration as constant. To compare quantitatively, the intrinsic binding constant K_b of complexes with ctDNA were determined according to the following equation, $[DNA]/(\varepsilon_a-\varepsilon_f) = [DNA]/(\varepsilon_b-\varepsilon_f) + 1/K_b(\varepsilon_a-\varepsilon_f)$, where, [DNA] is the concentration of DNA in base pairs, the apparent absorption coefficients ε_a, ε_f, and ε_b correspond to A_{obsd}/[complex], the extinction coefficient for the free complexes and the extinction coefficient for the complexes in the fully bound form, respectively. Double distilled water was used to prepare all buffer solutions.

The complexes did not show luminescence behaviour at room temperature in any of the organic solvents examined and in the presence of ctDNA. Hence, the fluorescence binding studies were performed using ethidium bromide (EB) as a reference to determine the

relative DNA binding properties of complexes with ctDNA in 5 mM Tris–HCl/ 5 mM NaCl buffer, pH 7.2. Fluorescence intensities of EB at 596 nm with an excitation wavelength of 515 nm were measured at different complex concentrations.

The DNA cleavage studies were performed by gel electrophoresis experiment using pBR322 plasmid DNA (which show clear DNA fragmentation pattern when compared to ctDNA). The cleavage activity was evaluated by monitoring the conversion of supercoiled plasmid DNA (Sc – form I) to nicked circular DNA (Nick- form II) and linear DNA (Lin – form III). Each reaction mixture was prepared by adding 2 μL (200 ng) of supercoiled DNA, 2 μL of 500 mM Tris – HCl/500 mM NaCl buffer (pH = 7.4), 4 μL of hydrogen peroxide and 6 μL of the complex dissolved in DMF. The final reaction volume was 20 μL, the final buffer concentration was 50 mM and the final concentration of complex varied between 100 and 200 μM. Samples were typically incubated for 1h at 37 ºC and after incubation, 5 μL of DNA loading buffer (0.25% bromophenol blue, 0.25% xylene cyanol, 30% glycerol in water) were added to each tube. The sample was then loaded onto a 0.8% agarose gel in TBE buffer (89 mM Tris-borate, 1.0 mM EDTA pH 8.4) containing ethidium bromide (0.5 μg/mL). Negative and positive controls were loaded on each gel electrophoresis and the experiment was carried out for 1.30 h at 50 V. The reaction was also carried out in the presence of KI (40 mM) (hydrogen peroxide scavenger), DMSO (40 mM) (hydroxy radical scavenger) and NaN_3 (40 mM) (singlet oxygen quencher).

2.6. Molecular docking

The molecular docking studies for all complexes were performed *in-silico* by using HEX 8.0 software [20]. The coordinates of nickel(II) complexes **1** and **5** were taken from their respective crystal structure as a CIF file and converted to the PDB format using Mercury 3.3 software (http://www.ccdc.cam.ac.uk/). The structures of complexes without single crystal data were sketched by CHEMSKETCH (http://www.acdlabs.com) and converted to

PDB format from MOL format by Mercury 3.3 software. The crystal structure of the B-DNA dodecamer d(CGCGAATTCGCG)$_2$ (PDB ID: 1BNA) was downloaded from the protein data bank (http://www.rcsb.org./pdb). All calculations were carried out on an Intel pentium4, 2.4 GHz based machine running MS Windows XP SP2 as the operating system. The docked pose of complex and DNA was visualized using CHIMERA software (www.cgl.ucsf.edu/chimera).

2.7. Antimicrobial screening

Antimicrobial activity of nickel(II) complexes **1** – **5** were tested against the bacterial species (*Staphylococcus aureus*, *Escherichia coli*, *Bacillus subtilis* and *Pseudomonas aeruginosa*) cultured on nutrient agar medium and against the fungal species (*Aspergillus niger* and *Candida albicans*) cultured on potato dextrose agar medium by the well-diffusion method. The medium preparation was detailed in the supplementary article. For the investigation of the antimicrobial activity, all the complexes were dissolved in dimethylsulfoxide (DMSO) to a final concentration of 100 μg/mL. The sample was filled into the wells of agar plates directly, incubated at 37 ^{o}C for 24 h for bacteria and 38 h for fungi. The diameter of the inhibition zone around each well was measured after the incubation period and studies were performed in duplicate. The solvent was also examined as a control to study the effect of DMSO (solvent) on the growth of microorganisms, which showed no inhibition.

3. Results and discussion

3.1. Synthesis and characterization

The synthesis of the nickel(II) complexes was done using a common procedure, by reaction of a stoichiometric amount of nickel chloride salts with the respective ligands in methanol as given in scheme 1. The analytical data obtained for complexes **1**–**5** were consistent with the formation of di-Schiff's base nickel(II) complexes. The obtained

complexes were insoluble in water, methanol, ethanol, and chloroform but soluble in acetonitrile, dimethylformamide (DMF) and DMSO. The lower molar conductivity values of complexes **1**–**4** showed the neutral non-electrolyte behaviour, and complex **5** with higher conductivity showed 1:2 electrolyte behaviour.

3.2. Crystal structure

Crystal data and details of the structure determination of complexes **1** and **5** were presented in Table 1, selected bond lengths and bond angles were listed in Table 2. Suitable crystals for the single crystal X-ray diffraction were grown by slow evaporation of complex dissolved in acetonitrile solvent. The ORTEP views shown in Figures 1 and 2 suggested the complex **1** with slightly distorted octahedral coordination geometry and complex **5** with distorted square-planar geometry. The X-ray structure of the complex **1** showed the hexacoordinated nickel(II) ion with two N, N, O donors of two Schiff's base ligand molecules in distorted octahedral geometry [18]. In the crystal structure of **1**, it was noticed that the basal plane is formed by the two N atoms of the azomethine group and the two O atoms of the phenolic hydroxyl group of salicylaldehyde moiety, where the nickel atom was in the equatorial plane of the octahedron. The axial positions of the distorted octahedron were observed to be occupied by the nitrogen atoms containing dimethyl groups in the Schiff's base ligand. The two 3-(dimethylamino)-1-propylamine ligands joined with nickel atom and form the chair conformation. The larger axial Ni–N1 and Ni–N3 distances of 2.302 Å, and 2.330 Å, respectively were observed for the complex **1**. The equatorial Ni–N2 and Ni–N4 bonds of the complex were observed to be (2.050 Å and 2.055 Å) greater than the equatorial Ni–O1 and Ni–O2 bonds (2.014(15) Å and 2.010(15)) [21].

The trans angles O1–Ni–O2, N1–Ni–N3 and N2–Ni–N4 is found to be 179.23(6), 179.82(7) and 179.77(8)º, respectively; and the cis angles N2–Ni–O2 and N4–Ni–O1 is present at 88.33(7) and 87.67(7)º, respectively. The trans and cis angles of the complex

deviate from 180º and 90º shows the presence of slight distortion in the octahedral structure of nickel(II) complex. The packing diagram of complex **1** (Figure S1) showed the intermolecular hydrogen bonding contacts formed at the para position to the carbon attached to azomethine nitrogen moiety. The hydrogen bonding also occurs between the two methyl groups of the adjacent molecule in crystal packing.

The crystal structure of complex **5** showed the four-coordinated nickel(II) ions with two N, O donors of two molecules of Schiff's base ligand in distorted square-planar geometry. The trans two O atoms coordinated to nickel atom with Ni1–O2 bond lengths of 1.830 Å and the two azomethine N atoms coordinated to nickel atom with Ni–N bond lengths of 1.897 Å. The cis angle N–Ni–O in the asymmetric unit in a plane with ligand molecule was 91.26° and out of a plane with ligand molecule was 91.26°; the trans angles N–Ni–O was found to be 180° between azomethine nitrogen one ligand and oxygen of another ligand molecule.

The one-half of the Schiff's base ligand molecule containing the 3-(dimethylamino)-1-propylamine unit and another half of the Schiff's base ligand with naphthaldehyde unit were observed above and below the N2O2N2O2 plane, both incline to the plane at an angle of 120.6° and 96.92°, respectively. The position of the ligand molecule causes a change in the cis angles of the coordination sphere and causes a slight distortion in the square planar geometry of the complex. The packing diagram of complex **5** (Figure S2) showed the intermolecular hydrogen bonding in the complex and weak intramolecular hydrogen interactions at H10B···H14 at 2.358(7) Å. The hydrogen bonding also observed between the two methyl groups of the adjacent molecule in crystal packing. The presence of interchain π–π stacking interactions extends the structure into an interesting 3D supramolecular array and stabilizes the packing of the complex in the crystal lattice.

3.3. Physico-chemical characterizations

The IR spectra of complexes **1–5** showed a sharp band in the region of 1619-1636 cm^{-1} attributed to ν(C=N) stretching vibration [22], which confirms the presence of Schiff's base in the complex. All complexes have bands in the region of 3070–3095 cm^{-1} and 2876–2895 cm^{-1}, which can be assigned to C–H stretching vibrations. Further evidence of coordination of ligands with the metal ions was revealed by the band at 456–622 cm^{-1} assigned to the metal-oxygen (M–O) vibration in all complexes [23].

The absorption spectral data obtained experimentally for all the nickel(II) complexes in DMF solution show peaks near 272 - 288 nm due to $\pi \rightarrow \pi^*$ transition of Schiff's base ligands. In the UV region of complexes **1**–**5**, broad/slightly intense peaks or a shoulder was observed in the region of 310–419 nm which could be assigned for the ligand to metal charge transfer transitions [24]. In the visible region of nickel(II) complexes **1**–**4**, the absorption bands near 538–653 nm and 695–745 nm can be attributed to $^3T_{2g} \leftarrow {}^3A_{2g}$ and $^3T_{1g}(F) \leftarrow {}^3A_{2g}$ transitions [25], which were consistent with the distorted octahedral geometry. The visible spectrum of complex **5** displayed the absorption bands below 670 nm characteristic of the spin allowed d–d transitions which have a low-spin d^8 nickel(II) ion in a square-planar environment. Thus, the absorption peak at 635 of nickel(II) complex **5** can be assigned to $^1A_{1g} \rightarrow {}^1A_{2g}$ [26], which strongly favours a square-planar geometry around the central metal ion.

The electron spray ionization (ESI) mass spectrum of nickel(II) complexes **2** and **4** (Figures S3&S4) showed their corresponding molecular ion peak at *m/z* 497.0 and *m/z* 558.7(6) assignable to $[Ni(\mathbf{L^2})_2+H]^+$ and $[Ni(\mathbf{L^4})_2+H]^+$, respectively. The base peaks at *m/z* 220.9(100) for complex **2** and at *m/z* 113.7 (100) for complex **4** were attributed to $[C_{13}H_{20}N_2O]^+$ and $[C_6H_{14}N_2]^+$ fragments. The ESI mass spectral data of the Schiff base nickel(II) complexes are in good agreement with the proposed structure of complexes.

3.4. Electrochemical studies

The molar conductivity of the freshly prepared complex in acetonitrile solution was observed to be 12-28 $\Lambda_m Scm^{-1}mol^{-1}$ indicating that the complexes **1**-**4** were neutral. The electrochemical behaviour of the nickel(II) complexes was studied in DMF solution using cyclic voltammetry in the potential range of +1.80 to -1.80 V containing 10^{-1} M tetra(n-butyl)ammonium perchlorate. The voltammetric data of nickel(II) complexes (scan rate 50 mV s^{-1}) were summarized in Table 3 and displayed in Figure 3. Controlled potential electrolysis performed at a potential 100 mV showed more negative than the reduction wave indicates the consumption of one electron per molecule.

The nickel(II) complexes showed a metal-centred quasi-reversible cyclic voltammetric response in the cathodic region as given in Table 3 due to the Ni(II)/Ni(I) couple. The ratio of cathodic to anodic peak height was less than one. However, the peak current increases with the increase of the square root of scan rates. From these data, it can be deduced that the redox couple was related to a quasi-reversible one-electron transfer process controlled by diffusion. The reduction potential of nickel(II) complexes were in the order **4** < **5** < **3** < **2** < **1**, suggesting that the electron donating/withdrawing groups influences on the electron density at the metal center, that tries to stabilize nickel(I) ions leading to easy reduction and shifts to a less negative potential [27, 28]. One quasi-reversible redox wave was observed at an anodic region which can be assigned to Ni(II)/Ni(III) [29].

3.5. DNA binding studies

3.5.1. Absorption spectroscopy

Absorption experiments were performed in UV-Visible spectroscopy by titrating the fixed concentrations of the complexes (40 μM) with an increase in the concentration of ctDNA (10 mM) at 25 ^oC. The absorbance of DNA itself was eliminated by adding equal amounts of DNA to both the complex solution and the reference solution. The intrinsic binding constant of complexes with ctDNA was determined by monitoring the absorption

intensity near 260 - 350 nm. Upon addition of increasing amount of ctDNA to complexes **1**–**5**, a significant "hypochromic" shift (8-39%) in the intra-ligand bands were observed near 260-350 nm accompanied by a redshift of 2–3 nm, indicative of stabilization of the DNA helix, which suggest that the complexes bind to DNA by intercalation.

The "hypochromic effect" may be due to the presence of planar aromatic chromophore that facilitates a strong binding interaction of the complexes with ctDNA thereby, providing an opportunity for the complex to bind with the ctDNA via partial insertion of the aromatic moiety in between the stacking base pair [30]. The spectrophotometric titrations of the complex **5** were shown in Figure 4 and other complexes **1**–**4** are shown in Figure S5. In plots of [DNA]/(ε_b–ε_f) vs [DNA], K_b is given by the ratio of the slope to the intercept. The K_b values obtained for nickel(II) complexes **1**–**5** were 1.50 × 10^4, 3.74 × 10^4, 4.02 × 10^4, 8.56 × 10^4, and 1.35 × 10^5 M^{-1}, respectively, following the order **5** > **4** > **3** > **2** > **1**. The complex containing 2-hnap was having higher binding affinity than that of complexes, this may be due to the better coplanarity and square planar geometry of the complex [31,32]. The binding constant K_b for the nickel(II) complexes **1**–**5** are in the range 10^3-10^5 M^{-1} were in good agreement with values of similar DNA intercalators [33, 34].

3.5.2. Fluorescence spectroscopy

The fluorescence spectroscopy technique is an effective method to study metal complex interaction with DNA. The addition of the complex to DNA pretreated with EB causes an appreciable reduction in the fluorescence intensity, indicating that complexes **1**–**5** compete with EB to bind with DNA. The reduction of the emission intensity gives a measure of the DNA-binding propensity of the complexes and stacking interaction between adjacent DNA base pairs [35]. The intensity of the emission band near 590 nm of the EB–DNA system decreased (up to 90% of the initial fluorescence intensity for **1**, up to 87% for **2**, up to 60% for **3**, up to 79% for **4** and up to 55% for **5**) upon addition of each complex **1**–**5** at

diverse r values (Figure S6). The emission spectra of EB bound to DNA in the absence and presence of complex **5** was shown in Figure 5 (complexes **1**–**4** are shown in Figure **S7**). According to the classical Stern–Volmer equation, $I_0/I = 1 + K_{sv}$ [Q], I_0 and I are the fluorescence intensities in absence and presence of quencher, respectively; K_{sv} is a linear Stern–Volmer quenching constant; [Q] is the concentration of the quencher.

The fluorescence quenching curve of DNA-bound EB by complexes **1**–**5** illustrated that the quenching of EB bound to DNA by complexes **1**–**5** was in good agreement with the linear Stern–Volmer equation. In the linear fit plot of I_0/I versus [complex]/[DNA], K_{sv} is given by the ratio of the slope to the intercept. The K_{sv} values for nickel(II) complexes **1**–**5** are 1.30×10^4 M^{-1}, 1.50×10^4 M^{-1}, 4.02×10^4 M^{-1}, 8.56×10^4 M^{-1} and 1.37×10^5 M^{-1}, respectively. The hydrophobic property of the rigid complex facilitates the DNA binding [36, 37]. The binding constant value obtained for the complexes were like that of other complexes with Schiff's base ligand, which reveals that the synthesized complexes have a good binding propensity. The K_{sv} values imply that all the complexes can strongly interact with DNA and are protected by DNA efficiently since the hydrophobic environment inside the DNA helix reduce the accessibility of solvent water molecules to the complex and the complex's mobility is restricted at the binding site [38].

3.6. Molecular docking studies

The complexes **1**−**5** were successively docked within the DNA duplex of sequence $d(CGCGAATTCGCG)_2$ dodecamer (PDB ID: 1BNA) in order to predict the chosen binding site along with the preferred orientation of the ligand inside the DNA. The minimum energy docked poses (Figure S8) revealed that complexes fitted into the curved contour of the targeted DNA in the minor groove and is situated within G–C/ A–T region, and slightly bends the DNA in such a way that a part planar aromatic rings make favorable stacking interactions between DNA base pairs leading to van der Waals interaction and hydrophobic

contacts with DNA functional groups that define the groove [39]. The resulting relative binding energies of docked metal complexes **1**–**5** with DNA were found to be –251.20, –279.51, –285.37, –270.21 and –337.85 Kcal/mol, respectively, which was also in accordance with *in-vitro* DNA binding studies, that the nickel complexes with 2-hydroxy-1-naphthaldehyde is more prominent DNA binder.

3.7. DNA cleavage studies

The DNA cleavage activities of nickel(II) complexes (**1**–**5**) have been studied by using supercoiled pBR322 plasmid DNA as a substrate in a medium of 50 mM Tris–HCl/50 mM NaCl buffer (pH = 7.4) in the presence of hydrogen peroxide (oxidizing agent). The control experiments with the ligand or metal salts or DNA alone do not reveal any significant cleavage. All the complexes do not show cleavage in absence of oxidizing agent even at a higher concentration.

The gel electrophoresis separations of plasmid pBR322 DNA by the nickel(II) complexes **1**–**5** in the presence of H_2O_2 was shown in Figure 6. The supercoiled form was converted to nicked circular form about 50% at 100 μM concentration of the complexes **1**–**5** (Figure 6, lanes 3–7 respectively) in the presence of H_2O_2. As the concentration of complexes increased to 200 μM, Form I was maximum converted to Form II and no linear form was observed (Figure 6, lanes 8–12). At 200 μM concentration of complex **5**, multiple scissions occur in a cleavage showing efficient cleavage (Figure 6, lane 12) compared to other nickel(II) complexes. The maximum cleavage was observed for complex **5** containing Schiff's base ligand of 2-hnap than that of other complexes. It shows that the presence of more aromatic, more planar ligand and geometry of the complex influence on the cleavage process [40 –42].

To establish the DNA cleavage mechanism of nickel(II) complexes, the cleavage of DNA was also further investigated in the presence and absence of scavengers DMSO, KI

(hydroxyl radical scavengers) and NaN_3 (singlet oxygen quencher) for oxidative species. The additives have no effect on DNA cleavage activity in control experiments (Figure 7a, lanes 3 and 9; Figure 7b, lane 3) which indicates their non-involvement in DNA cleavage activity. The result illustrated in Figure 7 shows no inhibition of cleavage process in the presence of DMSO (Figure 7a, lanes 4-8) and significant inhibition in the cleavage process in presence of KI (Figure 7a, lanes 10-14) indicating that hydroxyl radical was not involved in the cleavage process but hydrogen peroxide influence on the cleavage process. The addition of sodium azide (singlet oxygen quencher) inhibits the cleavage process (Figure 7b, lanes 4-8) indicating that $^1O_2$ was the activated oxygen intermediate and responsible for the cleavage of Ni(II) complexes. The significant increase in the DNA cleavage activity of nickel(II) complexes in the presence of H_2O_2 and the inhibition of activity in the presence of DMSO, KI and NaN_3 suggest that the cleavage was preferentially proceeded by the formation of singlet oxygen species [43].

3.8. Antimicrobial activity

The inhibition efficiencies of the complexes **1–5** were tested against two gram-negative (*Escherichia coli* and *Pseudomonas aeruginosa*) and two gram-positive bacteria (*Staphylococcus aureus* and *Bacillus subtilis*) and two fungal species (*Aspergillus niger* and *Candida albicans*) (Figures S9-11). The experimental result shown in Table 4 indicates that all the complexes exhibit higher inhibition efficiency, which can be explained based on chelate formation [40, 41]. The chelation reduces the polarity of ligand due to the overlap of the ligand orbital and partial sharing of the positive charge of the metal ion with donor groups. Further, it increases the delocalization of π-electrons over the whole chelate ring and enhances the lipophilic nature of the complexes. This increased lipophilicity enhances the transportation of the complexes into the lipid membrane and restricts further multiplicity of the microorganisms. By comparing the bacterial species, the complexes exhibit higher

inhibition efficiency for gram-positive bacteria than gram-negative bacteria. In fungal species, the complexes show greater activity for *C. albicans* than that for *A. niger* species.

The complex containing 2-hydroxy-1-naphthaldehyde appended Schiff base ligand has higher efficiency than other complexes with sal, msal, bsal and nsal as a substituent. This may be due to the presence of additional phenyl group and higher planarity in the complex containing a ligand with 2-hnap. The obtained results of complexes have also been compared with those of the standard drugs, amikacin and ketoconazole for bacteria and fungi, respectively. The complexes exhibited similar activities compared with the respective standard drugs.

4. Conclusions

The nickel(II) complexes were synthesized *in-situ* by using Schiff base ligands and characterized by physiochemical methods. The single crystal analyses, molar conductivity values and absorption studies confirm the distorted octahedral and distorted square-planar geometry of complexes **1** and **5**, respectively. The complexes showed efficient DNA binding following the order of **5** > **4** > **3** > **2** > **1**. The gel electrophoresis results for the complexes with plasmid DNA showed an oxidative (O_2-dependent pathway) cleavage in the presence of hydrogen peroxide by the hydroxy radical mechanism. All complexes showed a larger zone of inhibition for Gram-positive bacteria than that of Gram-negative bacteria. The 2-hydroxy-1-naphthaldehyde based Schiff base Ni(II) complex showed better results than other complexes due to its better electronic/steric property and square planar geometry. Thus, the above results evidenced that the steric factor influences the structural geometry, electronic properties, and biomolecular activity of the complex.

Supplementary material

Crystallographic data in CIF format for compounds **1** and **5** have been deposited at the Cambridge Crystallographic Data Centre, CCDC No. **1010002** and **949770**. Copies of

CIFs are available free of charge from The Director, CCDC, 12 Union Road, Cambridge, CB2 1EZ, UK (fax: -/44-1223-336-033; email: deposit@ccdc.cam.ac.uk or http://www.ccdc.cam. ac.uk). The mass spectra of complexes **2** and **4**; absorption, fluorescence spectral studies of complexes **1**–**4** are given in the supplementary material.

Acknowledgements

The authors thank the STIC, Cochin University of Science and Technology, Cochin for single crystal XRD and SAIF, Central Drug Research Institute (CDRI), Lucknow for analyzing the mass spectra.

References

[1] (a) A. Hazari, S. Giri, C. Diaz, A. Ghosh, Polyhedron 118 (2016) 70–80; (b) C.T. Lyons, T.D.P. Stack, Coord. Chem. Rev. 257 (2013) 528–540.

[2] (a) W.-B. Sun, B.-L. Han, P.-H. Lin, H.-F. Li, P. Chen, Y.-M. Tian, M. Murugesu, P.- F. Yan, Dalton Trans. 42 (2013) 13397–13403; (b) J. Cheng, X. Ma, Y. Zhang, J. Liu, X. Zhou, H. Xiang, Inorg. Chem. 53 (2014) 3210–3219.

[3] (a) H. Miyasaka, A. Saitoh, S. Abe, Coord. Chem. Rev. 251 (2007) 2622–2664; (b) O.A. El-Gammal, E.-R.G. Abu, S.F. Ahmed, Spectrochim. Acta, A 135 (2015) 227–240.

[4] (a) V.M. Leovac, D.M. Joksovic, V. Divjakovic, L.S. Jovanovic, Z. Saranovic, A. Pevec, J. Inorg. Biochem. 101 (2007) 1094–1097; (b) M. Hong, H. Geng, M. Niu, F. Wang, D. Li, J. Liu, H. Yin, Eur. J. Med. Chem. 86 (2014) 550–561.

[5] (a) T. Sedaghat, M. Yousefi, G. Bruno, H. Amiri Rudbari, H. Motamedi, V. Nobakht, Polyhedron 79 (2014) 88–96; (b) J.R. Anacona, N. Noriega, J. Camus, Spectrochim. Acta. A 137 (2015) 16–22.

[6] (a) S. Kundu, S. Biswas, A.S. Mondal, P. Roy, T.K. Mondal, J. Mol. Struct. 1100 (2015) 27-33; (b) S. Medici, M. Peana, V.M. Nurchi, J.I. Lachowicz, G. Crisponi, M.A. Zoroddu,

Coord. Chem. Rev. 284 (2015) 329–350; (c) N.P. Barry, P.J. Sadler, Chem. Commun. 49 (2013) 5106–5131.

[7] A.B. Gündüzalp, N. Ozbek, N. Karacan, Med. Chem. Res. 21 (2012) 3435–3444.

[8] M.C. Heffern, J.W. Kurutz, T.J. Meade, Chem. Eur. J. 19 (2013) 17043–17053.

[9] (a) M. Isloor, B. Kalluraya, K.S. Pai, Eur. J. Med. Chem. 45 (2010) 825–830; (b) M. Sebastian, M. Hissler, C. Fave, J. Rault-Berthelot, C. Odin, R. Reau, Angew. Chem. Int. Ed. 45 (2006) 6152–6155.

[10] P. Mukherjee, C. Biswas, M.G.B. Drew, A. Ghosh, Polyhedron 26 (2007) 3121–3128.

[11] H.L. Zhu, Y.X. Tong, X.M. Chen, C.X. Ren, Trans. Met. Chem. 26 (2001) 528–531.

[12] A. Elmali, C.T. Zeyrek, Y. Elerman, Z. Naturforsch., Chem. Sci. B 59 (2004) 228–232.

[13] C. Arici, F. Ercan, R. Kurtaran, O. Atakol, Acta Crystallogr., Sect. C: 57 (2001) 812–814.

[14] S.M.M. Sony, K. Saraboji, M.N. Ponnuswamy, J. Manonmani, M. Kandasamy, H.K. Fun, Cryst. Res. Technol. 39 (2004) 185–192.

[15] A. Jayamani, N. Sengottuvelan, G. Chakkaravarthi, Polyhedron 81 (2014) 764–776.

[16] L. Sacconi, P. Nannelli, U. Campigli, Inorg. Chem. 4 (1965) 818–822.

[17] L. Sacconi, P. Nannelli, N. Nadri, U. Campigli, Inorg. Chem. 4 (1965) 943–949.

[18] L. Sacconi, N. Nadri, F. Zanobini, Inorg. Chem. 5 (1966) 1872–1876.

[19] Bruker, *Bruker AXS Inc*, Madison, Wisconsin, USA, 2004.

[20] D. Mustard, D.W. Ritchie, Proteins: Struct. Funct. Bioinf. 60 (2005) 269–274.

[21] H.F. Qian, Y. Dai, J. Geng, L. Wang, C. Wang, W. Huang, Polyhedron 67 (2014) 314–320.

[22] P. Li, M. Niu, M. Hong, S. Cheng, J.M. Dou, J. Inorg. Biochem. 137 (2014) 101-108.

[23] T.M. Fasina, O.D. Olorunfemi, Pharma. Chemica 6 (2014) 18–22.

[24] H. Felora, R. Saeedi, A. H. Mona, A. Payam, N. Bernhard, Polyhedron 31 (2012) 443–450.

[25] P.K. Suganthy, R.N. Prabhu, V.S. Sridevi, Inorganica Chim. Acta 449 (2016) 127-132.

[26] B.S. Garg, D. Nandan Kumar, Spectrochim. Acta A, 59 (2003) 229–234.

[27] S.K. Mandal, L.K. Thompson, K. Nag, J.P. Charland, K.J. Gabe, J. Inorg. Chem. 26 (1987) 1391–1395.

[28] A. Jayamani, V. Thamilarasan, V. Ganesan, N. Sengottuvelan, P. Manisankar, S.K. Kang and Y-I. Kim, Spectrochim. Acta A 122 (2014) 365–374.

[29] W. Grochala, A. Jagielska, K. Wozniak, A. Wieckowska, R. Bilewicz, B.K. Daszkiewicz, J. Bukowska, L. Piela, J. Phys. Org. Chem. 14 (2001) 63–73.

[30] J.M. Chen, W. Wei, W.X.L. Feng, T.B. Lu, Chem. Asian J. 2 (2007) 710–714.

[31] B. Peng, H. Chao, B. Sun, H. Li, F. Gao, L.N. Ji, Inorg. Biochem. 100 (2006) 1487–1494.

[32] S. Anbu, M. Kandaswamy, Polyhedron 30 (2011) 123–131.

[33] (a) A. Zianna, G. Psomas, A. Hatzidimitriou, M.L. Kantouri, J. Inorg. Biochem. 163 (2016) 131-142; (b) A. Chylewska, M. Biedulska, M. Makowski, J. Mol. Liq. 243 (2017) 771-780.

[34] (a) S. Roy, P.K. Bhaumik, K. Harms, S. Chattopadhyay, Polyhedron 75 (2014) 57–63. (b) M. Dehkhodaei, M. Khorshidifard, H.A. Rudbari, M. Sahihi, G. Azimi, N. Habibi, S. Taheri, G. Bruno, R. Azadbakht, Inorganica Chim. Acta 466 (2017) 48-60.

[35] N. Raman, K. Pothiraj, T. Baskaran, J. Coord. Chem. 64 (2011) 3900–3917.

[36] E. Nyarko, N. Hanada, A. Habib, M. Tabata, Inorganica Chim. Acta 357 (2004) 739–745.

[37] Y. Zhao, J. Zhu, W. He, Z. Yang, Y. Zhu, Y. Li, J. Zhang, Z. Guo, Chem. Eur. J. 12 (2006) 6621–6629.

[38] M. Shakira, S. Khanam, M. Azam, M. Aatif, F.J. Firdaus, J. Coord. Chem. 64 (2011) 3158–3168.

[39] S. Tabassum, A. Asim, F. Arjmand, M. Afzal, V. Bagchi, Europ. J. Med. Chem. 58 (2012) 308–316.

[40] R. Sanyal, S.K. Dash, P. Kundu, D. Mandal, S. Roy, D. Das, Inorganica. Chim. Acta 453 (2016) 394–401.

[41] S.M. Pradeepa, H.S.B. Naik, B.V. Kumar, K.I. Priyadarsini, A. Barik, S. Jayakumar, Inorganica. Chim. Acta 428 (2015) 138–146.

[42] N. Mahalakshmi, R. Rajavel, Arab. J Chem. 7 (2014) 509–517.

[43] P. Arthi, A. Haleel, P. Srinivasan, D. Prabhu, C. Arulvasu, A.K. Rahiman, Spectrochim. Acta A 129 (2014) 400–414.

[44] (a) C.T. Yang, B. Moubaraki, K.S. Murray, J.J. Vittal, Dalton Trans. (2003) 880–889; (b) M. Rajasekar, S. Sreedaran, R. Prabu, V. Narayanan, R. Jegadeesh, N. Raaman, A. Kalilur Rahiman, J. Coord. Chem. 63 (2010) 136–146.

[45] M. Asadi, K.A. Jamshid, A.H. Kyanfar, Inorganica. Chim. Acta 360 (2007) 1725–1730.

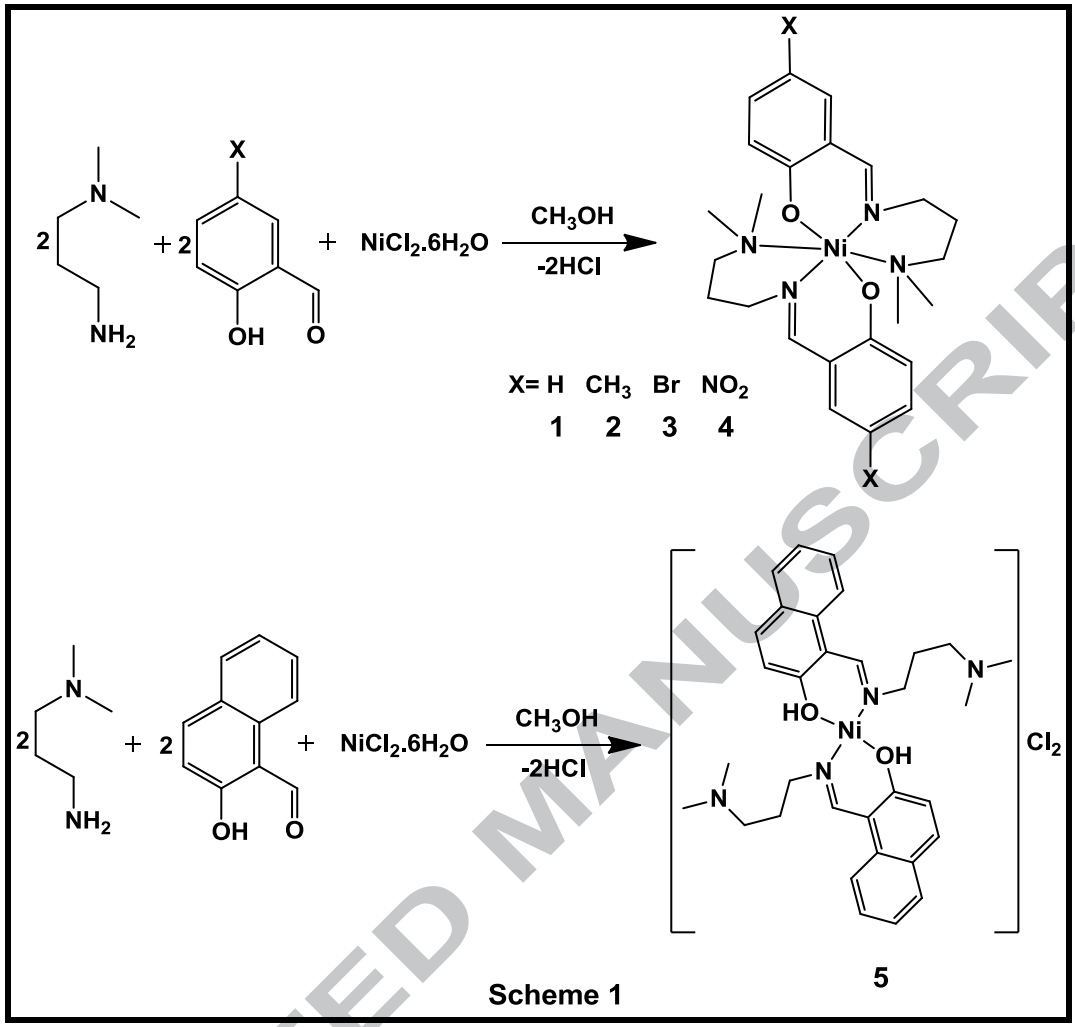

Scheme 1

Table 1. Crystallographic data and structure refinement parameters for complexes **1** and **5**

	1	**5**
Empirical formula	$C_{24}H_{34}N_4NiO_2$	$C_{32}H_{38}N_4NiO_2.Cl_2.2H_2O$
Formula weight	496.26	569.36
Temperature (K)	293(2)	296(2)
Wavelength (Å)	0.71073	0.71073
Crystal system, space group	Monoclinic, P_21/c	Monoclinic, P_21/c
a (Å)	10.2312(6)	12.5721(4)
*B(*Å)	15.3327(9)	10.8367(4)
c (Å)	15.3774(8)	12.2393(4)
α (°)	90	90
β (°)	107.0350(10)	95.522(2)
γ (°)	90	90
Volume ($Å^3$)	2306.4(2)	1659.74(10)
Z, calculated density (mg m^{-3})	4, 1.351	2, 1.353
Absorption coefficient (mm^{-1})	0.869	0.787
F(000)	1000	712
Crystal size (mm)	0.30 × 0.25 × 0.20	0.35 × 0.30× 0.25
Theta range for data collection (°)	1.92 to 25.00	1.63 to 28.32
Limiting indices, *h,k,l*	$-12 \le h \le 12$, $-18 \le k \le 18$, $-17 \le l \le 18$	$-16 \le h \le 15$, $-14 \le k \le 14$, $-16 \le l \le 11$
Reflections collected/ unique	31264/ 4057	12672 / 4063
*R*int	0.0303	0.0248
Data / restraints / parameters	4057 /0 / 280	4063 / 3 / 207
Goodness-of-fit on F^2	1.137	0.704
Final R indices [$I > 2\sigma(I)$]	R1 = 0.0310, wR2 = 0.0759	R1 = 0.0423, wR2 = 0.1391
R indices (all data)	R1 = 0.0454, wR2 = 0.0887	R1 = 0.0626, wR2 = 0.1768
Largest difference peak and hole / e $Å^{-3}$	0.724 and –0.196	0.729 and –0.331

Table 2. Selected bond lengths (Å) and bond angles (°) for **1** and **5**

1		**5**	
Ni(1) -N(1)	2.302(19)	Ni(1)-O(2)#1	1.8302(14)
Ni(1) -N(2)	2.050(17)	Ni(1)-O(2)	1.8302(14)
Ni(1) -N(3)	2.329(18)	Ni(1)-N(2)	1.8971(18)
Ni(1) -N(4)	2.055(18)	Ni(1)-N(2)#1	1.8971(18)
Ni(1) -O(1)	2.014(15)	O(2)#1-Ni(1)-O(2)	180.00(10)
Ni(1) -O(2)	2.010(15)	O(2)#1-Ni(1)-N(2)	88.74(7)
O(2)-Ni(1)-O(1)	179.2(6)	O(2)-Ni(1)-N(2)	91.26(7)
O(2)-Ni(1)-N(2)	88.3(7)	O(2)#1-Ni(1)-N(2)#1	91.26(7)
O(1)-Ni(1)-N(4)	87.67(7)	O(2)-Ni(1)-N(2)#1	88.74(7)
N(2)-Ni(1)-N(4)	179.76(8)	N(2)-Ni(1)-N(2)#1	179.999(1)
O(2)-Ni(1)-N(3)	87.55(7)		
N(1)-Ni(1)-N(3)	179.82(7)		

Table 3. Electrochemical data of nickel (II) complexes

Complexes	At cathodic region				At anodic region			
	E_{pc} (V)	E_{pa} (V)	$E_{1/2}$ (V)	ΔE (mV)	E_{pa} (V)	E_{pc} (V)	$E_{1/2}$ (V)	ΔE (mV)
1	-0.81	-0.58	-0.70	230	+1.06	+0.88	+0.97	180
2	-0.84	-0.61	-0.73	230	+1.16	+1.06	+1.11	100
3	-0.79	-0.62	-0.71	170	+1.51	+1.34	+1.42	170
4	-0.69	-0.51	-0.60	180	+1.14	+1.04	+1.09	100
5	-0.84	-0.67	-0.76	170	+1.20	+1.03	+0.98	170

Table 4. Antimicrobial activities of salen type di-Schiff base nickel (II) complexes **1**–**5**

Complex	Zone inhibition diameter (mm)					
	Bacteria				Fungi	
	Gram-negative		Gram-positive		*A. niger*	*C. albicans*
	E. coli	*P. aeruginosa*	*B. subtilis*	*S. aureus*		
1	15	9	15	17	10	19
2	14	15	15	16	12	12
3	12	14	13	12	13	13
4	14	13	15	13	14	14
5	16	15	15	14	14	16
Amikacin	18	17	18	18	NT	NT
Ketokonazole	NT	NT	NT	NT	19	19

Figure captions

Figure 1. 30% probability ORTEP diagram of complex **1**. Hydrogen atoms are omitted for clarity.

Figure 2. 30% probability ORTEP diagram of complex **5**. Hydrogen atoms are omitted for clarity.

Figure 3. Cyclic voltammograms of di-Schiff base nickel(II) complexes **1**–**5** for (a) Reduction process & (b) Oxidation process

Figure 4. Absorption spectra of nickel(II) complex **5** (10^{-5} M) in 5 mM Tris–HCl/20 mM NaCl buffer at pH 7.2 in the absence and presence of increasing amounts of ctDNA Inset: plot of [DNA]/[ε_a- ε_f] vs. [DNA].

Figure 5. Emission spectra of EB bound to ctDNA in the presence of complex **5**. The inset shows the plot of I_0/I vs [DNA]/[complex].

Figure 6. Cleavage of SC pBR322 DNA (0.2µg, 33.3 µM) by Ni(II) complexes **1**–**5**(100µM, 200µM) in the presence of the H_2O_2 (100 µM) in 50 mMTris–HCl/50mM NaCl buffer (pH 7.2). Lane 1, DNA control; lane 2, DNA + H_2O_2; lanes 3–7, DNA + H_2O_2 + **1- 5** (100µM), respectively; lanes 8–12, DNA + H_2O_2 + **1-5** (200µM), respectively.

Figure 7. Cleavage of SC pBR322 DNA (0.2µg, 33.3 µM) by Ni(II) complexes **1**–**5** (100µM) in the presence of H_2O_2 (100 µM), hydroxyl radical scavengers (DMSO–40 mM, KI–40 mM) and singlet oxygen scavenger (NaN_3–40 mM) in 50 mMTris–HCl/50mM NaCl buffer (pH 7.2). (a) Lane 1, DNA control; lane 2, DNA + H_2O_2; lane 3, DNA + H_2O_2 + DMSO; lanes 4–8, DNA + H_2O_2 + DMSO + **1- 5** (100µM), respectively; lane 9, DNA + H_2O_2 + KI; lanes 10-14, DNA + H_2O_2 + KI + **1- 5** (100µM), respectively. (b) Lane 1, DNA control; lane 2, DNA + H_2O_2; lane 3, DNA + H_2O_2 + NaN_3; lanes 4–8, DNA + H_2O_2 + NaN_3 + **1- 5** (100µM), respectively.

Highlights

- di-Schiff base nickel(II) complexes prepared by *insitu* condensation & complexation
- Complexes presented good binding propensity to ctDNA
- Complex with bulky substituent showed square planar geometry and greater DNA interaction
- The nickel(II) complexes showed efficient cleavage of plasmid DNA

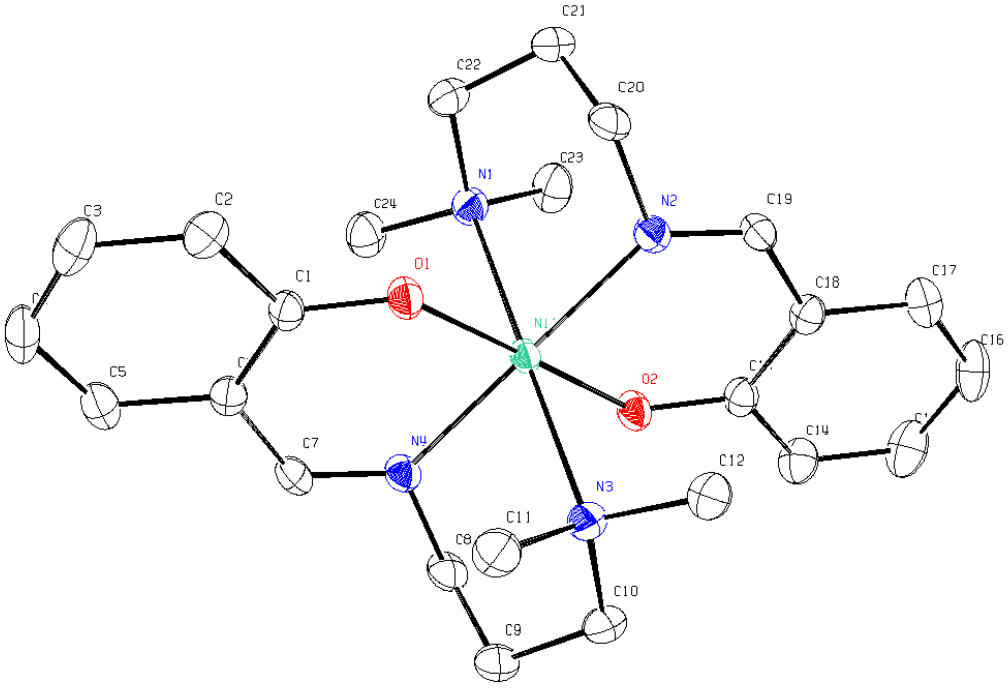

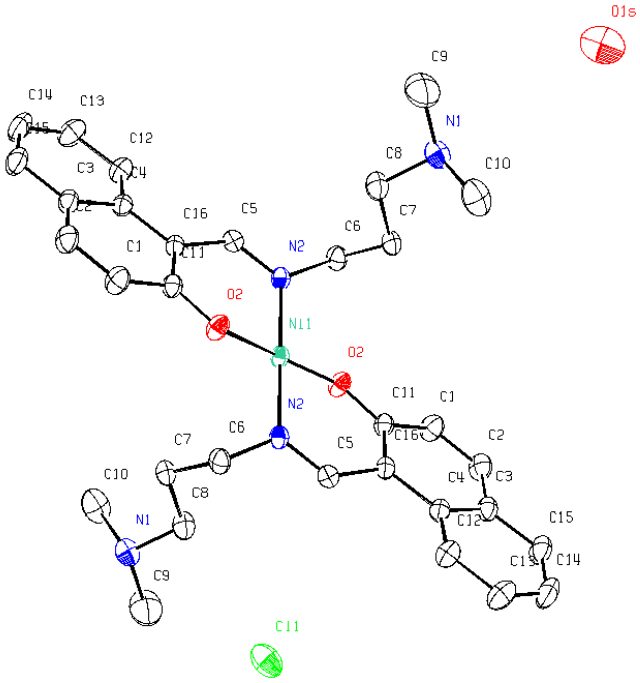

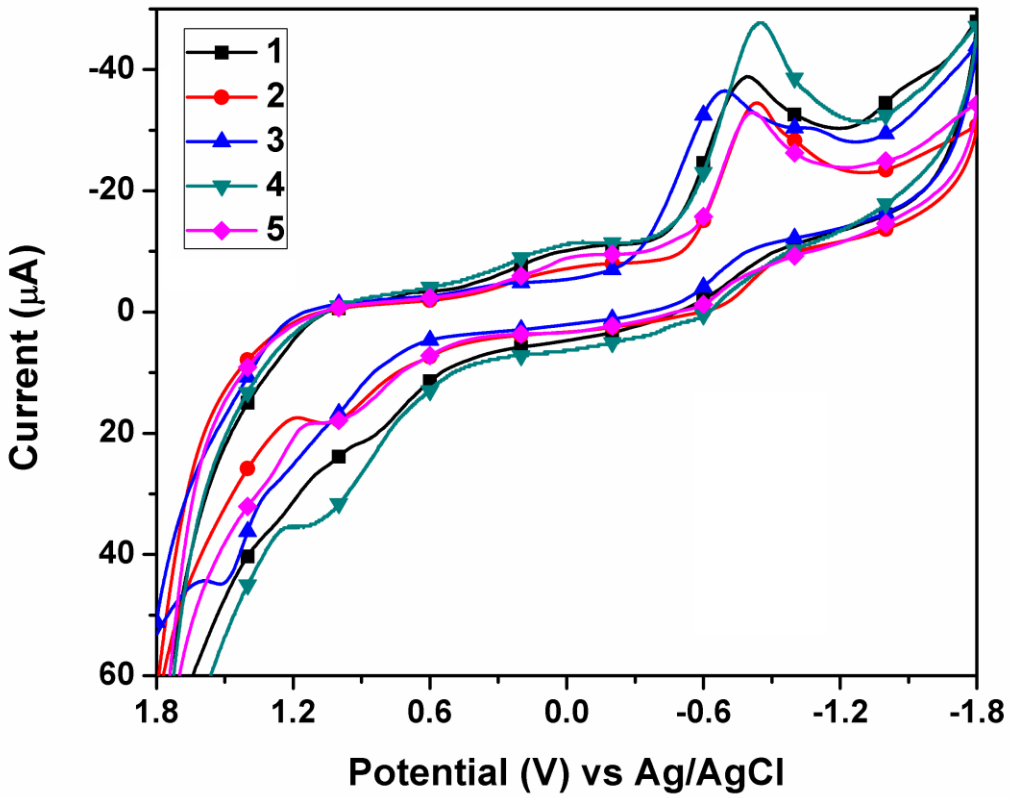

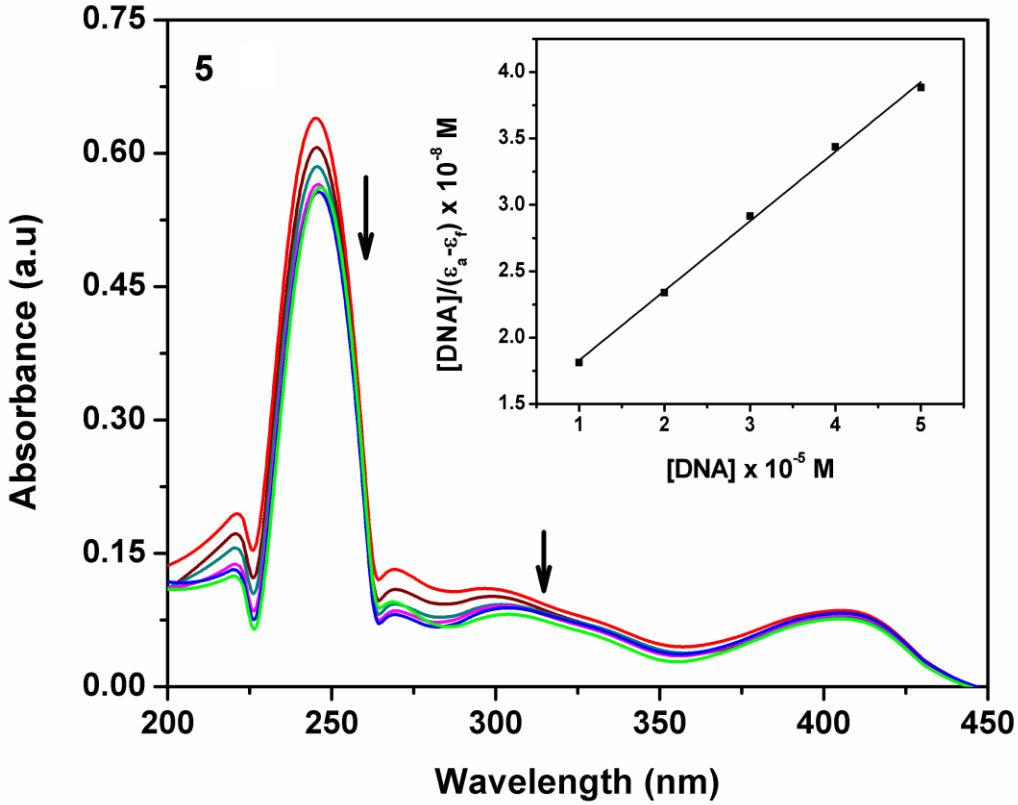

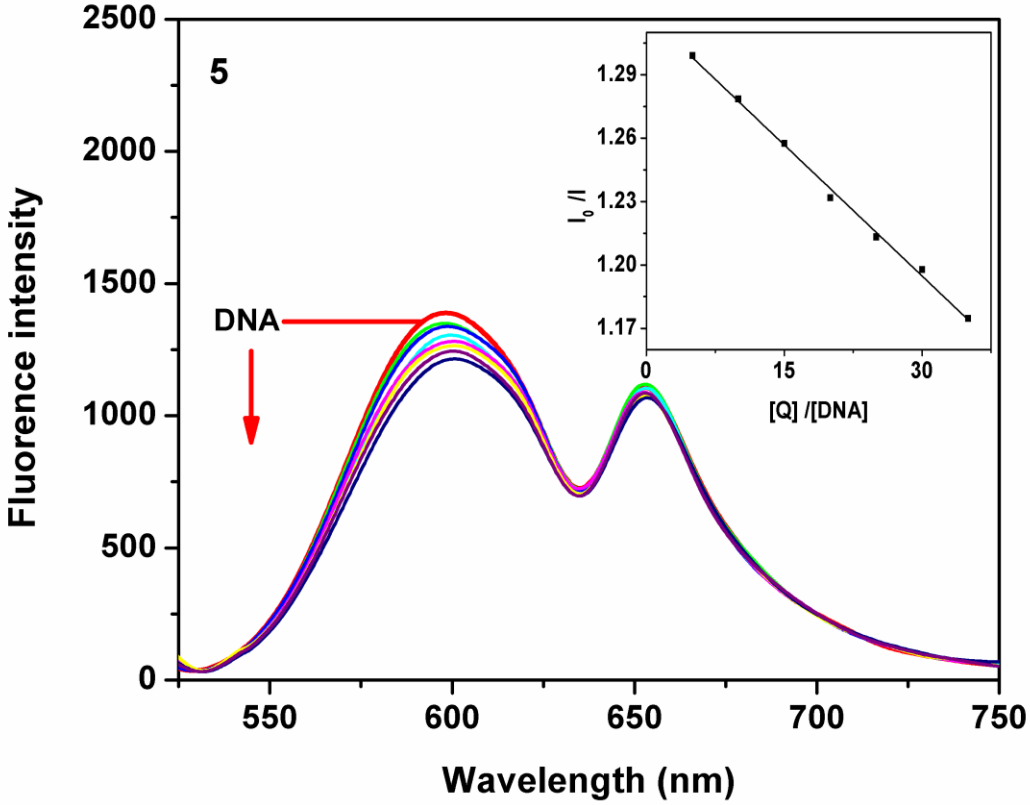

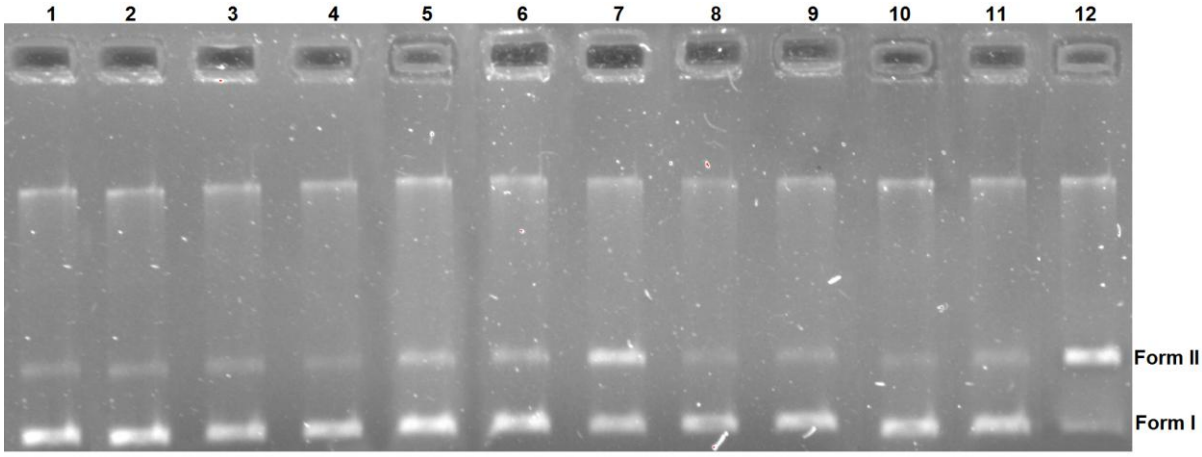

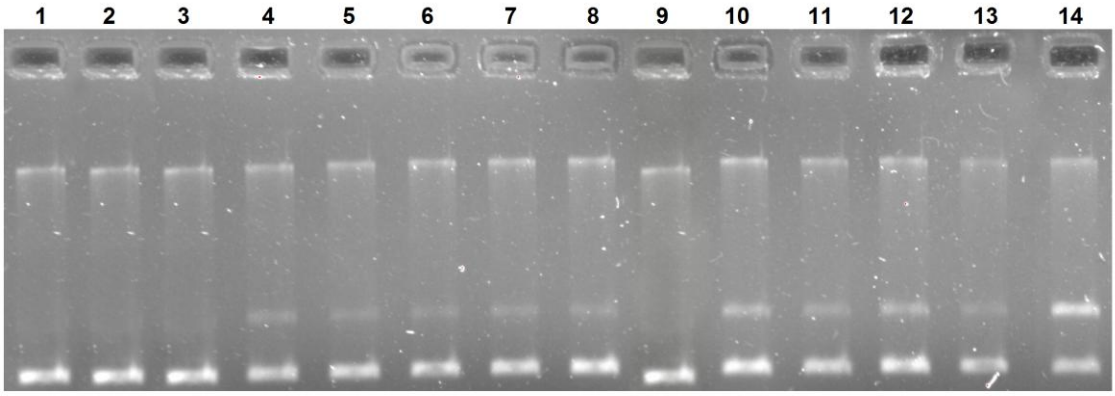

(a)

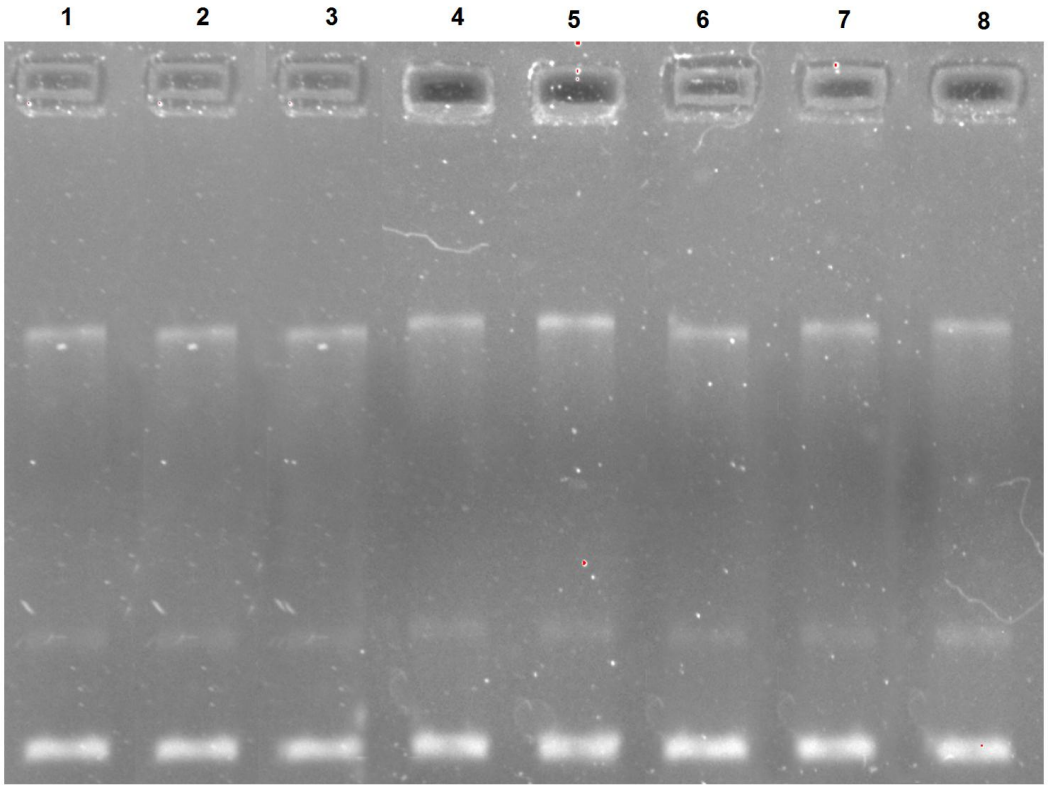

(b)

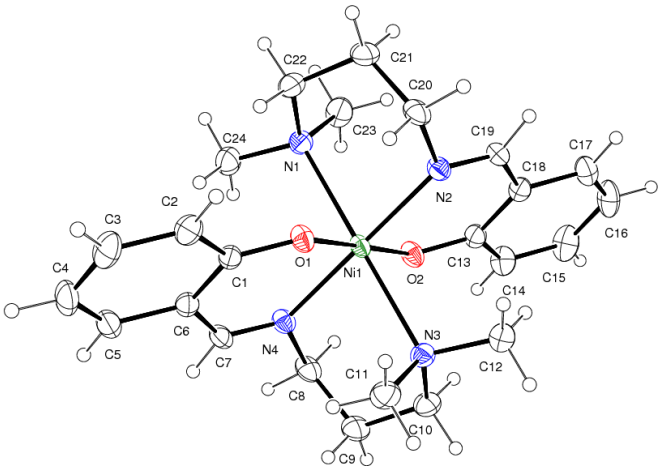

Nickel(II) complex 1

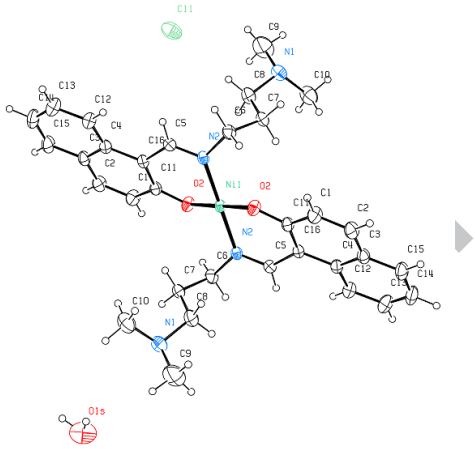

Nickel(II) complex 5